GPS Solut (2016) 20:9–21
DOI 10.1007/s10291-014-0435-z

ORIGINAL ARTICLE

Wide-area ionospheric delay model for GNSS users in middle- and low-magnetic-latitude regions

An-Lin Tao · Shau-Shiun Jan

Received: 8 November 2013 / Accepted: 18 December 2014 / Published online: 1 January 2015

Abstract A useful ionospheric delay model to compensate for the effect of ionospheric error on GNSS service over continent-wide areas or oceans is the Satellite-Based Augmentation System's wide-area thin-shell planar fit ionospheric grid model. In order to implement a proper wide-area ionospheric delay model in the Asia-Pacific region to reflect the variation introduced by local ionospheric activity, the present study develops a proper ionospheric delay model to correct ionospheric error in middle- and low-magnetic-latitude regions. Specifically, the proposed ionospheric delay model uses several dual-frequency GNSS reference stations distributed in Taiwan, South Korea, Japan, and China as grid points in place of the conventional grid points generated by ionospheric pierce points. The ionospheric delays observed at the reference stations are processed and provided to the user, who can then construct the ionospheric delay model using weighted least squares with the distances between the user and the stations as weights. This proposed ionospheric delay model lowers the computation load by eliminating the conversion of delays at the ionospheric pierce points to those at the grid points and provides good descriptions of dynamic variations due to the ionospheric activities. Also, a simplified model is developed to further reduce its computation load while providing almost the same service as that of the original proposed model. A selection mechanism between the original proposed model and its simplified version is developed as well. The details of the proposed ionospheric delay model are explained, and experiments conducted using data collected from the reference stations in the Asia-Pacific region are presented. The effectiveness of the proposed model is validated by comparison with the conventional wide-area thin-shell planar fit ionospheric grid model provided by the Japanese Multi-functional Satellite Augmentation System under both nominal and disturbed ionospheric conditions.

Keywords Global navigation satellite system (GNSS) · Satellite-based augmentation system (SBAS) · Ionospheric delay models

A.-L. Tao · S.-S. Jan (✉)
Department of Aeronautics and Astronautics, National Cheng Kung University, Tainan 70101, Taiwan
e-mail: ssjan@mail.ncku.edu.tw

Introduction

Global Navigation Satellite Systems (GNSS) provide position, time, and velocity information to users on or near the earth. Ionospheric activities, which are caused by solar radiation, influence GNSS signal propagation and can cause inaccurate user positioning solution. GNSS thus cannot be used for safety-of-life applications. In order to reduce the GNSS error caused by the ionosphere and protect users, GNSS augmentation systems have been developed, such as the Satellite-Based Augmentation System (SBAS) (Tsai et al. 1995). SBAS uses a thin-shell planar fit ionospheric delay model to remove the ionospheric delay for GNSS users with integrity information (Chao et al. 1996). However, SBAS only provides ionospheric grids in five-degree resolution, which is insufficient for users in low-magnetic-latitude regions such as the Asia-Pacific region (Kan 2005).

The present study develops a proper ionospheric delay model to correct the ionospheric error for GNSS users in low-magnetic-latitude areas, especially the Asia-Pacific region. In Fig. 1, we use GPS data obtained from the SOPAC IGS reference stations (RSs) to illustrate the

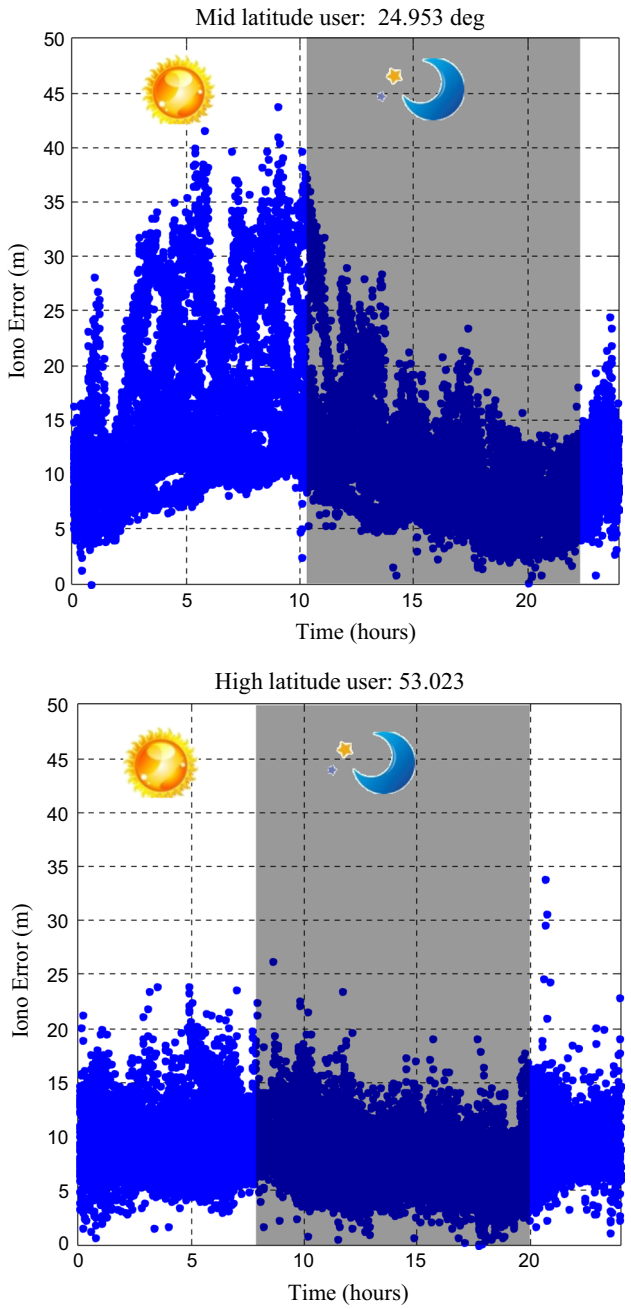

Fig. 1 Ionospheric delay variation during 1 day for users at various magnetic latitudes (mid-latitude user site code: TWTF, and high-latitude user site code: PETS)

ionospheric delays in different areas during March 3, 2012. The upper plot shows that the mid-latitude user (site: TWTF, longitude: 120.8932, latitude: 24.953°) experiences large variations in ionospheric delay, and the lower plot shows that high-latitude user (site: PETS, longitude: 158.668, latitude: 53.023°) experiencing smoother ionospheric delay. The ionosphere changes severely in low-magnetic-latitude areas, but the SBAS ionospheric model might give a constant value to users in a given five-degree longitude and latitude region (Kan 2005; Macalalad et al. 2013). In order to capture the dynamic variation of the ionosphere, we develop a thin-shell dynamic planar fit model. The model employs four dual-frequency GNSS RSs distributed geometrically in Taiwan. Ionospheric thin-shell models use the obliquity factor (OF) to convert the slant ionospheric delay into a vertical delay, which is then used to calculate the correction for the user (Chao et al. 1996).

Due to the difference between the two-dimensional (2D) thin-shell model and the actual three-dimensional ionosphere, an OF error is generated when the vertical ionospheric delay is converted into a slant ionospheric delay (Allain and Mitchell 2010; Radicella and Nava 2002; Radicella et al. 2004). As a result, the proposed model utilizes two methods to generate ionospheric corrections for the user, with the results verified with the true ionospheric delay value. The main difference between the two methods is that one uses OF and one does not. Both methods use ionospheric delays observed by the four RSs as scattered sample points to provide ionosphere corrections to users. In order to evaluate the positioning performance of the proposed ionospheric model, the Japanese Multi-functional Satellite Augmentation System (MSAS) is used as the baseline. Two experiment fields are used to validate the proposed ionospheric delay model. In the first experiment field, the RSs and users are distributed over Taiwan area. In the second experiment field, the RSs and user are distributed in Taiwan, South Korea, Japan, and China (i.e., Asia-Pacific region). In addition, the ionospheric activity has an 11-year cycle, and 2012–2013 being at the peak value. This study thus also examines the feasibility of the developed model under this circumstance.

We first describe the mathematical equations and algorithms of the proposed ionospheric delay model and then detail the experiment setup, including the hardware and software architectures, of the ionospheric delay model. Experimental results are also analyzed and discussed. Finally, conclusions and suggestions for future work are presented.

Ionospheric delay estimation

The ionosphere is a major error source for single frequency GNSS users. In order to compensate for ionospheric effects, several approaches have been proposed for single frequency GNSS users. For example, single frequency GNSS users could either rely on the ionosphere model, e.g., Klobuchar ionospheric model, built by the parameters contained in the navigation message or ionospheric delay corrections provided by some reference network to reduce the ionospheric effect. In this work, we focus on the latter approach and

propose an improved ionospheric delay model such that user positioning could be possibly improved.

Introduction to ionospheric delay

The ionosphere is a layer of the atmosphere that is approximately 50–1,000 km above the surface of the earth. The ionospheric delay value is directly proportional to the total electron content of the ionosphere, which is related to the magnetic latitude and time (Parkinson and Spilker 1996). The ionospheric delay thus varies with location and time. The ionospheric effects are largest for satellites near the horizon, and lowest for those in zenith direction. Moreover, the ionospheric delay is a function of the carrier frequency. The ionospheric delay can be estimated using dual-frequency GPS observations. The ionospheric delay calculated from a reference GPS station can be applied to build an ionospheric delay model, which is then used to calculate the ionospheric correction for users. The following section describes the correction algorithm and the process used to build an ionospheric model.

Parameter description of ionospheric correction

The first step of generating an ionospheric model is to calculate the ionospheric delay of each RS equipped with an L1–L2 dual-frequency receiver. The use of code pseudoranges (P) and carrier measurements (ϕ) of GPS signal with L1 and L2 frequencies is readily found in the literature. The first ionospheric correction obtained using dual-frequency observations is as follows,

$$I_{\mathrm{L1},P} \equiv \frac{P_{\mathrm{L2}} - P_{\mathrm{L1}}}{\gamma - 1} = I_{\mathrm{L1}} + v_P \tag{1}$$

$$I_{\mathrm{L1},\phi} \equiv \frac{\phi_{\mathrm{L1}} - \phi_{\mathrm{L2}}}{\gamma - 1} = I_{\mathrm{L1}} + N + v_\phi \tag{2}$$

where I_{L1} is the ionospheric delay at frequency L1, $I_{\mathrm{L1},P}$ is the combination of L1 and L2 code phase measurements, $I_{\mathrm{L1},\phi}$ is the combination of L1 and L2 carrier phase measurements, and γ is a constant (=1.647). N is the combination integer ambiguity for the carrier phase. Noise term v includes the multipath error, receiver thermal noise error, and other unpredictable errors. The terms N, v_P, and v_ϕ make the ionospheric delays calculated in (1) and (2) inaccurate. To reduce these errors and minimize noise, the Hatch filter is utilized for ionospheric delays (Hatch1982).

Ionospheric Hatch filter

This research utilizes the Hatch filter as a smoothing filter to estimate the smoothed ionospheric delay. For the ionospheric Hatch filter, the dual-frequency code and carrier ionospheric measurements, i.e., $I_{\mathrm{L1},P}$ and $I_{\mathrm{L1},\phi}$ in (1) and (2) are combined to obtain a better estimate of the ionospheric correction. The smoothing technique takes advantage of each measurement; that is, the mean value of $I_{\mathrm{L1},P}$ is close to the true ionospheric delay, and the result of $I_{\mathrm{L1},\phi}$ is smoother than that of $I_{\mathrm{L1},P}$. However, the code phase pseudorange is noisier than the carrier phase pseudorange, and the result of $I_{\mathrm{L1},\phi}$ is not accurate due to N. Two types of measurements could be used in a complementary fashion to improve ionospheric delay estimate, and the Hatch filter is therefore used as the smoothing algorithm as follows,

$$I_{\mathrm{smooth}} = \frac{1}{M} I_{\mathrm{L1},P} + \frac{M-1}{M}\left(I_{\mathrm{smooth,Last}} + I_{\mathrm{L1},\phi} - I_{L1,\phi,\mathrm{Last}}\right) \tag{3}$$

where I_{smooth} is the smoothed result of the dual-frequency carrier smoothing algorithm, M is the time constant, and the subscript *Last* is the data of the previous epoch. As a result, the ionospheric delay I_{smooth} is accurate and smooth. After smoothing, I_{smooth} is considered as the true ionospheric delay for the satellite to the dual-frequency receiver of the RS.

Ionospheric thin-shell model

In order to provide users with ionospheric corrections, an ionospheric delay model must be utilized. The proposed ionospheric delay model is similar to that of SBAS, which uses a 2D ionospheric thin-shell model to provide corrections (WAAS MOPS 2006),

$$\mathrm{OF} = \frac{\text{slant delay}}{\text{vertical delay}} = \left\{1 - \left[\frac{R_e}{R_e + h}\cos(el)\right]^2\right\}^{-\frac{1}{2}} \tag{4}$$

$$I_{\mathrm{vertical}} = \frac{I_{\mathrm{slant}}}{\mathrm{OF}} \tag{5}$$

First, the SBAS RS estimates the ionospheric slant delay at the ionospheric pierce point (IPP) and uses the satellite elevation angle to calculate the OF, as shown in (4). Then, the OF is used to calculate the vertical ionospheric delay at the IPP as shown in (5). Next, the vertical ionospheric delay at the IPP is taken to accumulate and generate the vertical ionospheric delay for each ionospheric grid point (IGP). Users can apply the ionospheric corrections at the IGPs to calculate the ionospheric corrections for their GPS observations. The provided corrections are vertical ionospheric delays. Users need to use the satellite elevation angle to calculate the OF, which is then used to calculate the slant ionospheric delays.

Proposed ionospheric delay model

Figure 2 shows an example location of IGPs in the Taiwan region. The blue circles are the locations of SBAS IGPs,

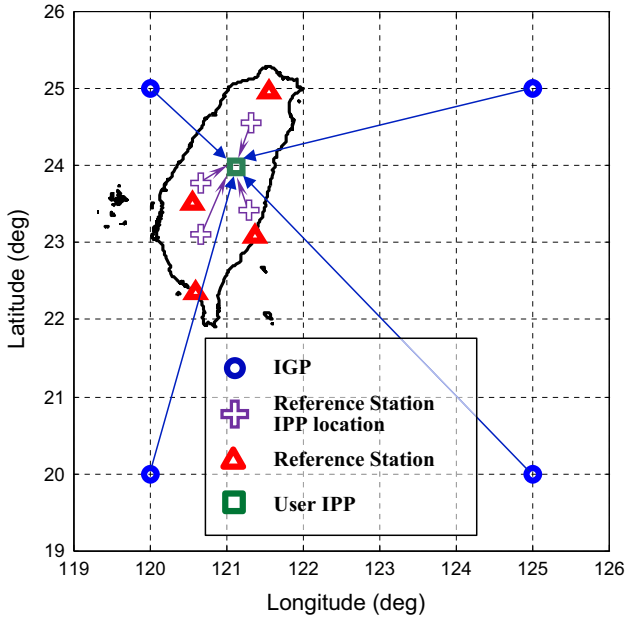

Fig. 2 Example SBAS IGP locations around Taiwan

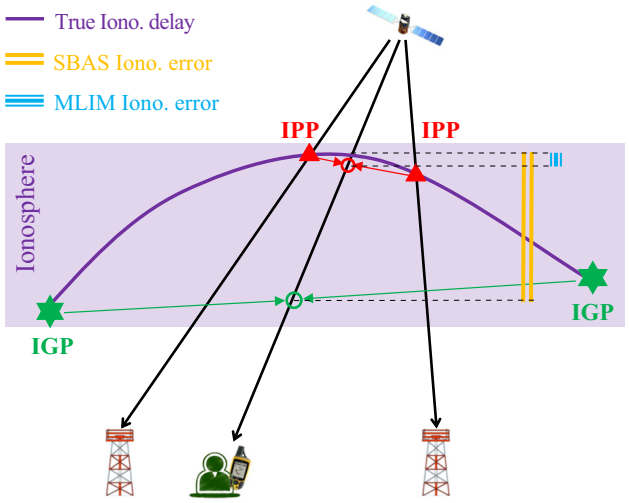

Fig. 3 Correction comparison of SBAS ionospheric model and MLIM

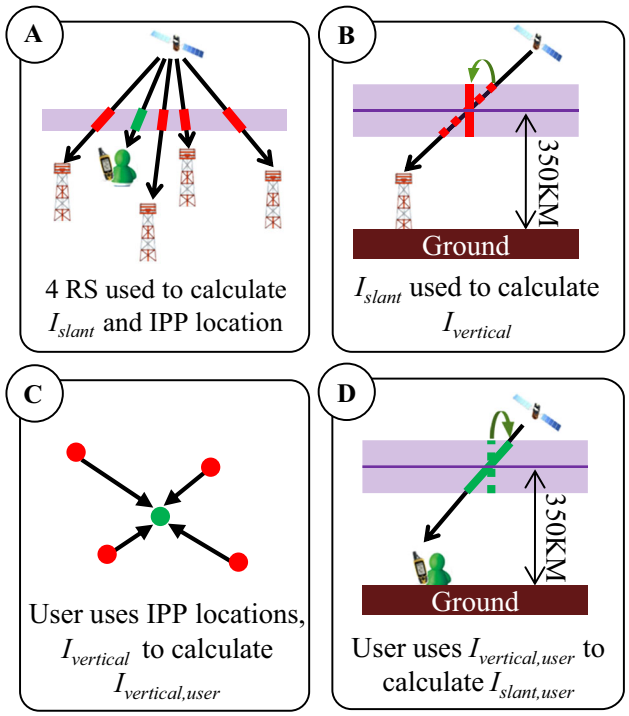

Fig. 4 Flowchart of building and using the MLIM with Method A

the purple crisscross marks are the locations of RS IPPs for a specific satellite at a specific epoch, the red triangles are the RSs, and the green square is the user IPP location. The proposed ionospheric delay model utilizes the IPP locations calculated from each RS instead of those of fixed IGPs to estimate the user ionospheric delays using WLS for each satellite. The distance between the user IPP and the RS IPP is regarded as the weight in WLS. For users in low-magnetic-latitude areas, after calculating the ionospheric delay at the RSs, this accurate information will be diluted when the process goes through the IGP algorithm. As a result, the ionospheric correction from SBAS is not as accurate as the original ionospheric delay at the RS. Figure 3 shows a case of the ionospheric delay value changing dramatically within 5° of latitude or longitude. The distance between the user and the pre-defined five-degree IGP of SBAS is too far to properly model the ionospheric delay within this region (Chen and Jan 2008). The figure indicates that users will receive more accurate ionospheric delay corrections when utilizing the proposed ionospheric delay model, because the RS IPPs capture a detailed variation of the ionospheric delay. The main difference between the proposed middle- and low-magnetic-latitude ionospheric model (MLIM) and the conventional ionospheric model is the ionospheric delay correction information. Specifically, the conventional ionospheric model provides ionospheric correction information for grid points. On the other hand, the MLIM provides the ionospheric correction information directly on the IPPs. As a result, the MLIM not only simplifies the processes of ionospheric delay correction but also improves the accuracy of the ionospheric delay modeling.

We propose two methods for building the proposed MLIM. The results of these two methods are compared in the following section. Figure 4 shows how the ionospheric delay model generates the correction for the user. In Fig. 4a, four RSs implement the dual-frequency carrier smoothing algorithm to calculate the ionospheric delay and IPP location for each satellite. In Fig. 4b, the OF is used to

compute the vertical ionospheric correction. In Fig. 4c, the user receives the ionospheric corrections from the four RSs for each satellite, and the distance between the RS IPP and the user IPP is used as the weight value to calculate the vertical ionospheric correction for the user using the WLS algorithm. Finally, Fig. 4d shows the user using the OF to transform the vertical ionospheric correction into slant ionospheric correction. The user thus removes the ionospheric delay. The first method is called the "Method A" in the remaining sections.

The design objective of the proposed ionospheric delay model is to reduce the computation load of the original model and maintain a more accurate ionospheric delay correction for users. Thus, we simplify the process of using the OF. The OF induces the error when vertical ionospheric delay is converted into slant ionospheric delay. This OF error depends on the satellite elevation angle, satellite azimuth, user latitude, solar activity, and season (Radicella and Nava 2002; Radicella et al. 2004). The magnitude of the OF error thus varies. For a given user located at a certain area and time, the major cause of OF inaccuracy is the low satellite elevation angle. The idea of the second method for constructing the MLIM, called the Method B, in the remaining sections, is depicted in Fig. 5. In Fig. 5a, four RSs implement the dual-frequency carrier smoothing algorithm to calculate the ionospheric delay for each satellite. In Fig. 5b, the user receives the slant ionospheric corrections from the four RSs for each satellite and uses them to calculate the slant ionospheric correction using WLS. The user then directly uses this slant correction to correct the ionospheric error.

In summary, the two proposed ionospheric delay models generate ionospheric corrections for users to remove ionospheric delays from GPS observations. For the normal case, the Method A is suggested to be applied to generate the ionospheric corrections because the Method A has better performance when the separation distance between two RSs is large. The selection mechanism between the two methods will be discussed in the next section.

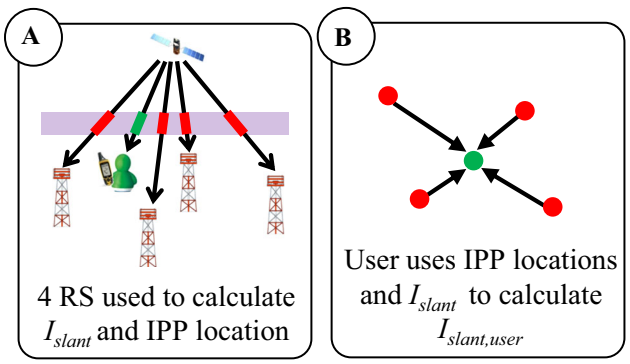

Fig. 5 Flowchart of building and using the MLIM with Method B

Experiment results and analyses

In the following, we use real GPS data to quantify the enhancement in performance of the MLIM. Two experiments are used for the RS networks and users. For the first experiment, we take the GPS data during March 5, 2012, in Taiwan to test the MLIM under the normal (undisturbed) ionosphere condition. The second experiment uses the GPS data collected in China, South Korea, Japan, and Taiwan on October 2, 2013, to evaluate the MLIM under disturbed ionosphere condition as well as its performance in Asia-Pacific region. As noted in the introduction, one objective is to quantify the enhancement in performance of using the MLIM relative to the SBAS model (WAAS MOPS 2006). Therefore, we use the real SBAS data from Japanese MSAS for both experiments to investigate the performance gain of the MLIM in comparison with the SBAS model under different ionosphere conditions.

Experiment setup

There are two groups of the GPS RSs and users used in this section. The first group analyzes the MLIM performance under the normal ionospheric activity day in Taiwan area, and the second group evaluates the accuracy of the MLIM under the severe ionospheric activity day in China, South Korea, Japan, and Taiwan (Asia-Pacific region). In addition, in order to verify the long-range ionospheric correction capability of the MLIM, the separation distances between the user and RSs for the second group are from 680 to 1,680 km. Thus, the wide-area ionospheric correction performance of the MLIM could be validated by the second experiment.

Experiment setup for Taiwan area

In the first experiment in Taiwan, the receivers operated by the National Land Surveying and Mapping Center of Taiwan were used as RSs to build the ionospheric delay model. The locations of users and the four RSs are depicted in Fig. 6. Each RS is equipped with a dual-frequency GPS receiver (Trimble NetRS) identical to the one used by the user. All receivers were set to provide GPS observations in RINEX data format (Gurtner 2007). The precise locations of North Reference Station (NRS), West Reference Station (WRS), South Reference Station (SRS), East Reference Station (ERS), and the users are given in earth-centered, earth-fixed (ECEF) coordinates (Enge 2001) in Table 1. We analyze the 24-h data collected from the four stations on March 5, 2012. The Kp index indicates the magnitude of geomagnetic disturbance on a 0–9 scale, for which the Kp index value over five presents the geomagnetic activity is active (Bartels, 1949). In this research, if the Kp index is

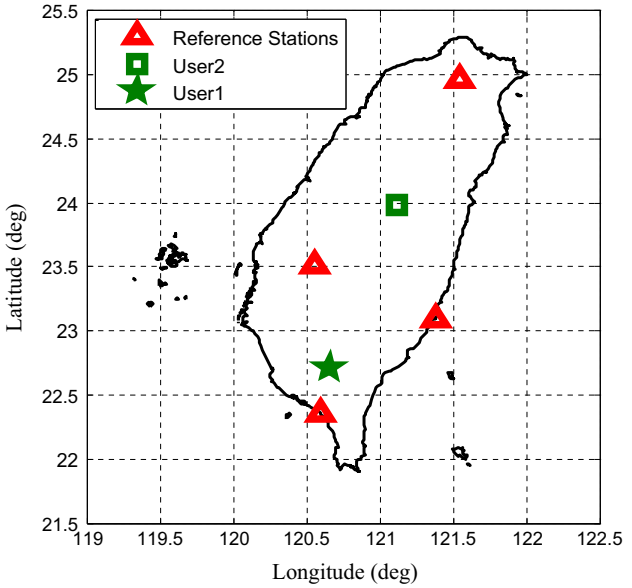

Fig. 6 Distribution of users and reference stations for experiment in Taiwan

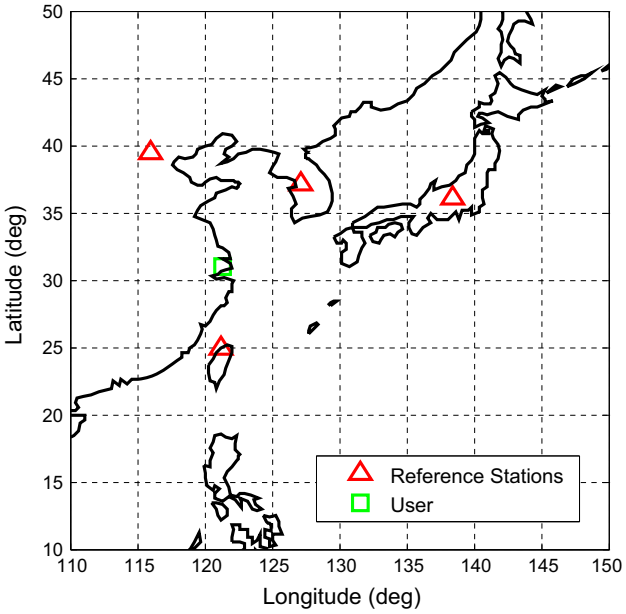

Fig. 7 Distribution of users and reference stations for experiment in Asia-Pacific region

Table 1 Known ECEF coordinates of users and reference stations used in the first experiment

	X (m)	Y (m)	Z (m)
NRS	−3,026,623.863	4,930,812.606	2,675,764.649
WRS	−2,974,175.645	5,039,606.451	2,529,050.706
SRS	−3,003,414.792	5,079,792.164	2,411,880.907
ERS	−3,056,055.600	5,011,630.323	2,486,770.031
User1	−3,013,835.460	4,992,843.369	2,577,671.971
User2	−3,001,266.923	5,064,358.730	2,446,967.148

<5, then the ionospheric activity is normal (undisturbed). If the Kp index is equal or larger than 5, then the ionospheric activity is severe (disturbed). The Kp index value generated every 3 h and the eight Kp values provided by GeoForschungsZentrum on March 5, 2012, were: 3−, 2, 2, 2+, 1+, 2−, 3−, and 3+. The eight Kp values of March 5, 2012, indicate that the ionosphere was under normal condition for that day.

Two user locations were used to analyze the wide-area correction capability of the proposed ionospheric model in Taiwan. As shown in Fig. 6, User 1 is close to SRS, and User 2 is far away from all RSs (in the middle of Taiwan).

Experiment setup for Asia-Pacific area

This second experiment extends to include the SOPAC IGS RSs in China, South Korea, Japan, and Taiwan. The GPS data are obtained from receivers in the SOPAC IGS RSs, and all receivers provided GPS observations in the RINEX data format. The experiment is to analyze the user positioning result for 24 h on October 2, 2013. The eight Kp values for this day were: 5+, 8−, 6−, 4−, 3, 3+, 6−, and 5-. These Kp values indicate an ionospheric storm on that day. The locations of RSs and the user are depicted in Fig. 7, and the precise locations in ECEF coordinate are given in Table 2. Table 3 provides a comparison table to show the separation distance between the user and RSs for the first experiment group and the second experiment group, and it is noted that separation distances are much larger for the second experiment than that of the first experiment. That is, the enlarged separation distance between the RSs and the user is to examine the wide-area correction performance of the MLIM.

In the following section, we will first validate the selection mechanism of the Method A and Method B for MLIM. We then compare the SBAS ionospheric delay model and the MLIM using the first experiment setup. The MLIM with the Method A was used to analyze the result in this part because the Method A is more robust than the Method B. Finally, the second experiment setup is used to verify the wide-area correction capability of the proposed ionospheric model under a severe ionospheric activity.

Algorithm selection of the proposed ionospheric model

This section focuses on the correction results obtained using the Method A and Method B. In general, if the user is far from a RS, the Method B will not generate proper corrections. Therefore, at the end of this section, the

Table 2 Known ECEF coordinates of users and reference stations used in the second experiment

	X (m)	Y (m)	Z (m)
NRS	−3,062,023.544	4,055,449.044	3,841,819.211
WRS	−2,148,743.366	4,426,640.803	4,044,656.794
SRS	−2,994,434.012	4,951,320.979	2,674,505.696
ERS	−3,855,263.036	3,427,432.557	3,741,020.293
User1	−2,831,733.583	4,675,665.958	3,275,369.410

Table 3 Separation distances between users and reference stations

	First Group (in Taiwan)		Second group (in Asia Pacific)
	User1	User2	User
NRS	266.131	116.762	870.958
WRS	89.913	78.254	1,058.439
SRS	38.391	187.498	680.804
ERS	85.827	101.974	1,680.039

Units are km

limitations of the Method B are analyzed. Only the results for User 1 in the first experiment setup are present here because the GPS data continuity of this user is better than that of the other users. The theoretical architecture of the Method A provides more complete information than that of Method B. However, as is shown later (Fig. 11), when the separation distance between user and the RSs is <285 km, the Method A can be reduced to the Method B, and by doing so, the computation load could be reduced and the correction accuracy could also be maintained at the same time.

Dual-frequency carrier smoothing of ionospheric delay value

The ionospheric correction from each RS for each satellite was calculated using a Hatch filter smoothing algorithm. In order to present the results of this correction obtained using the ionospheric delay model, Fig. 8 shows PRN 9 to demonstrate the ionospheric delay after the smoothing technique. The red, blue, and green lines are $I_{L1,P}$, $I_{L1,\phi}$, and $\hat{I}_{L1,smooth}$, respectively. It can be seen that $\hat{I}_{L1,smooth}$ integrates the advantages of $I_{L1,\phi}$ and $I_{L1,P}$, namely the trend and accuracy, respectively. The user uses this ionospheric correction to calculate the ionospheric delay. In the figure, the ionospheric delay changes with the elevation angle and time. The main factor that influences the ionospheric delay is the elevation angle. A high elevation angle has a small ionospheric delay. Ionospheric activity becomes more stable as the local time approaches nightfall.

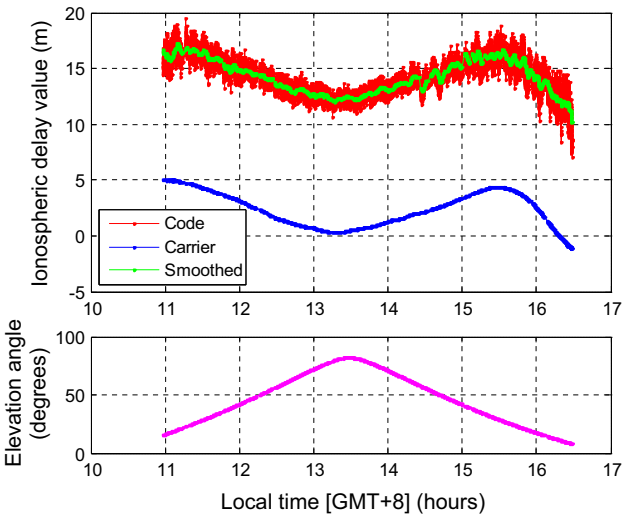

Fig. 8 PRN 7 ionospheric delay after smoothing technique

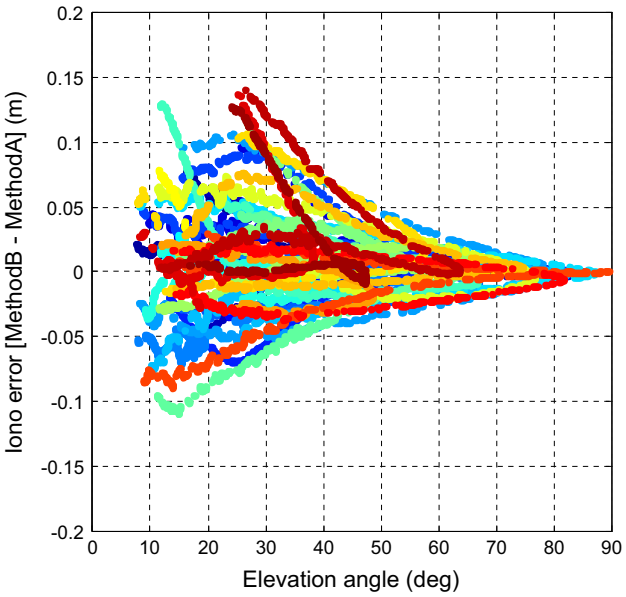

Fig. 9 Ionospheric correction difference between Method A and Method B

At nightfall, the ionospheric delay value is small regardless the elevation angle.

Correction error for method A and method B

The experiment results shown in Fig. 9 were obtained using the same data; only the method of generating the ionospheric correction is different (i.e., Method A and Method B). The results show that the ionospheric corrections produced by the two methods are different. The colors represent results from different satellites. The difference is larger at low elevation angles, but still within ±15 cm.

Moreover, the impact of this slight difference on the positioning result is small. As a result, this section will not compare the user positioning result by using the different methods, because the result is almost the same.

In order to verify which method is more accurate, the corrections obtained using the two methods (Method A and Method B) were compared with the true ionospheric delay (calculated from the dual-frequency measurement). Figure 10 shows the mean and standard deviation of the correction error for intervals of 5° elevation. For example, the point at a 20° elevation angle is the average data in the interval of 15–20°. The red, blue, and green points are the ionospheric correction errors obtained using the Method A and Method B, and the difference between the two methods, respectively. A green point above zero indicates that the error of the Method B is larger than that of the Method A. In general, the Method A has better accuracy. The difference between two methods at low elevation angles (0–30°) is not obvious. The results show that the error caused by the simplification is almost the same as the error caused by the OF. For a satellite at a middle elevation angle (30–50°), the correction of the Method A is more accurate, which means that the OF in this interval provides a better estimation. At high elevation angles, the two methods have similar accuracies. In summary, the Method A is more robust than the Method B. However, the corrections obtained from the two methods are almost identical.

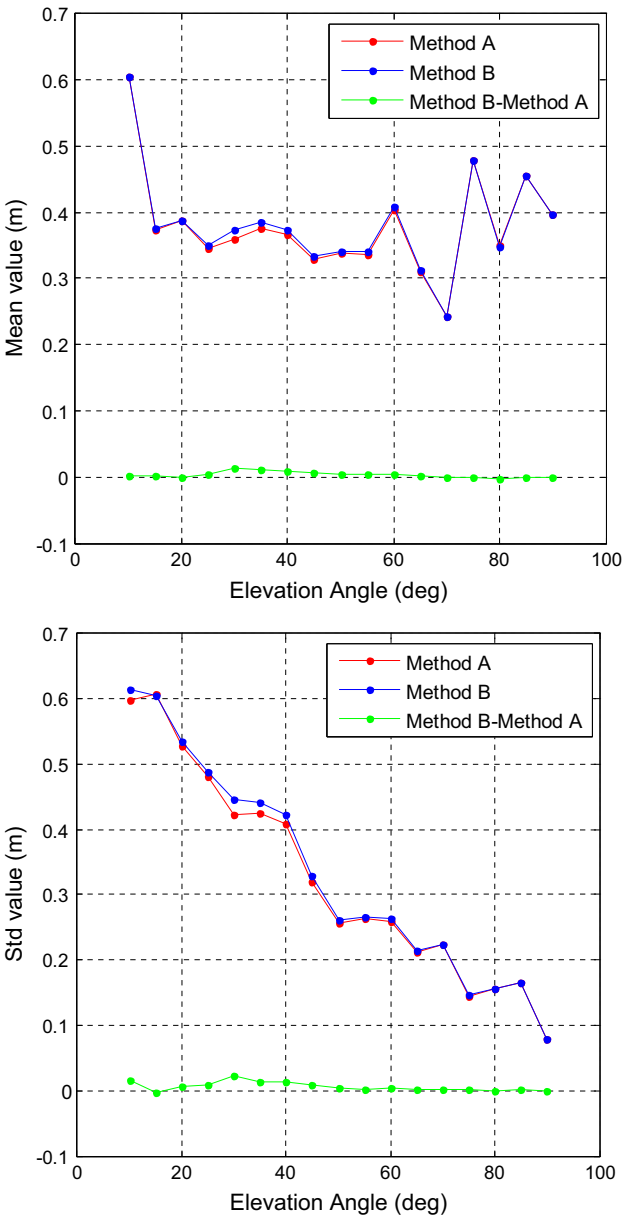

Fig. 10 Mean and standard deviation values of ionospheric correction error for Method A and Method B

Applicability analysis of method B

A simplified ionospheric delay model is proposed in this section to reduce the calculation time and to maintain the accuracy of the resulting ionospheric delay corrections. As noted earlier, the Method B does not require the calculation of OF. The Method B assumes that the ionospheric delay values for the same satellite from different RSs are the same. Therefore, the ionospheric delay value can be directly applied to WLS to generate the ionospheric correction for the user. In the previous section, we showed that the Method A and Method B produce almost identical results. However, when the RSs are further away, the ionospheric corrections from different RSs exhibit relatively large differences. In order to set up a mechanism to check the applicability of the Method B, all GPS observation stations were used to find a spatial correlation between the separation distance and ionospheric delay difference. All six GPS observation stations were used, including the two users. First, two of the stations were selected and the distance between them was calculated. Then, the ionospheric delay difference between these two stations and all satellites was calculated. The results for all 15 combinations of two stations were calculated. Figure 11 shows the standard deviation value of the ionospheric delay difference for the 15 combinations (blue points). The results show that ionospheric delay difference grows linearly with distance. These results were used to generate the following linear equation (red line) for the user to select the RS:

$$I_{1\sigma,\text{error}} = 6.47623 \times 10^{-6} \cdot D + 0.15 \quad (6)$$

where D is the distance in meters between the user and the RS. $I_{1\sigma,\text{error}}$ is the standard deviation of the ionospheric difference.

Our research shows that one could use Method B to generate the ionospheric delay correction only if the

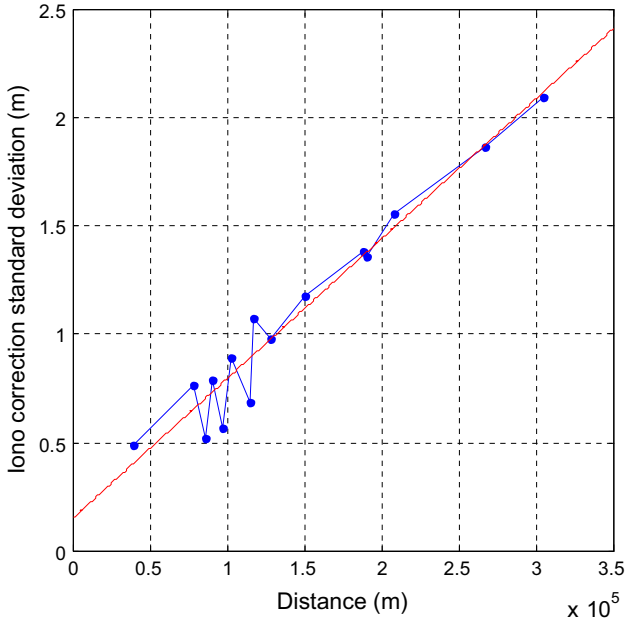

Fig. 11 Ionospheric delay difference between reference stations versus distance between two stations

ionospheric delay differences between the RSs and the user are <2 m. Thus, according to (6), in order to effectively apply Method B, the maximum distance between the user and RS is 285 km. For the general case, we suggest the Method A to be used for the MLIM.

Comparison of SBAS ionospheric delay model with proposed ionospheric delay model

In this section, the smoothed ionospheric correction and ionospheric delay values generated by each RS are compared with the SBAS ionospheric model. Then, the correction values for the two users are compared. Finally, the positioning results of the two users are compared.

Analysis of ionospheric correction

In order to validate the ionospheric delay value from each RS, a comparison study of the true and estimated ionospheric delay values was conducted. The true ionospheric delays at the user location were calculated from user's dual-frequency observations using the dual-frequency carrier smoothing algorithm. The estimated ionospheric corrections for satellite PRN 26 at locations of Users 1 and 2 are shown in Fig. 12. PRN 26 was selected to verify the ionospheric delay values because its elevation angle covers the whole range. The figure shows that for the two users, the trends of ionospheric corrections are the same. The corrections from MSAS are not as accurate as those of the reference stations.

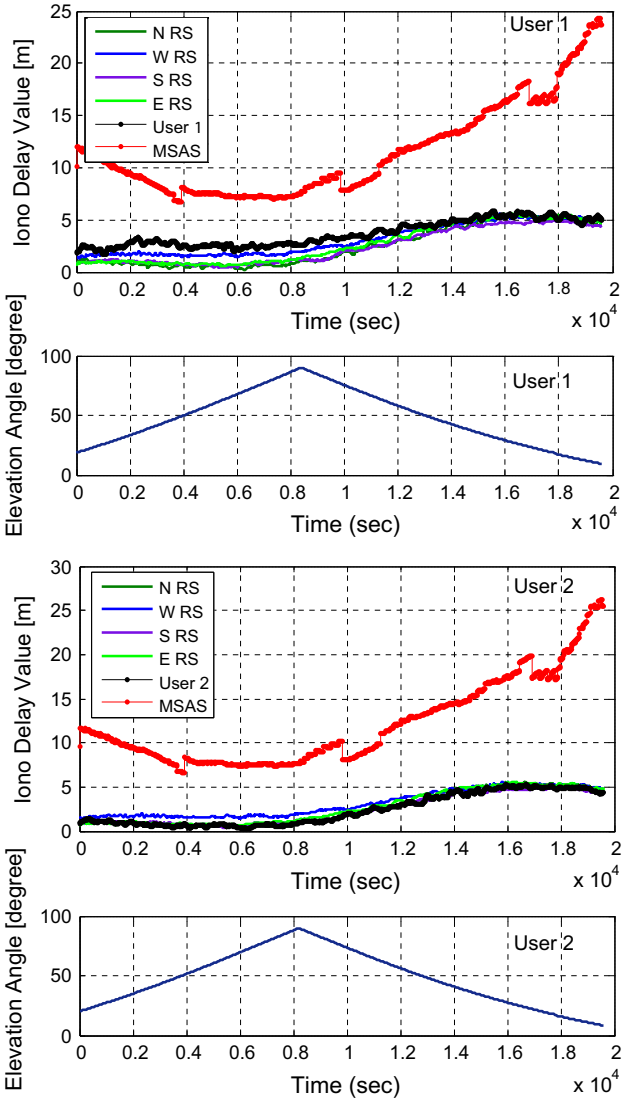

Fig. 12 Estimated ionospheric delays of users from reference stations, MSAS ionospheric model, and users dual-frequency receivers (truth)

In order to further analyze the ionospheric correction, Fig. 13 depicts the differences in ionospheric delays between the SBAS model and the proposed model and the true ionospheric delay. The true ionospheric delays are calculated directly from user L1-L2 dual-frequency GPS observations after the dual-frequency carrier smoothing algorithm. The results shown in the figure are the ionospheric delays for all satellites in-view over a whole day. These results are combined from all different satellites at different time periods so that the ionospheric delay results could be compared over a whole day, and the data sampling rate is 1 Hz. The lower subplot shows the corresponding elevation angles for these in-view satellites at different time periods over a whole day. By comparing all these results, one notes that the proposed ionospheric delay

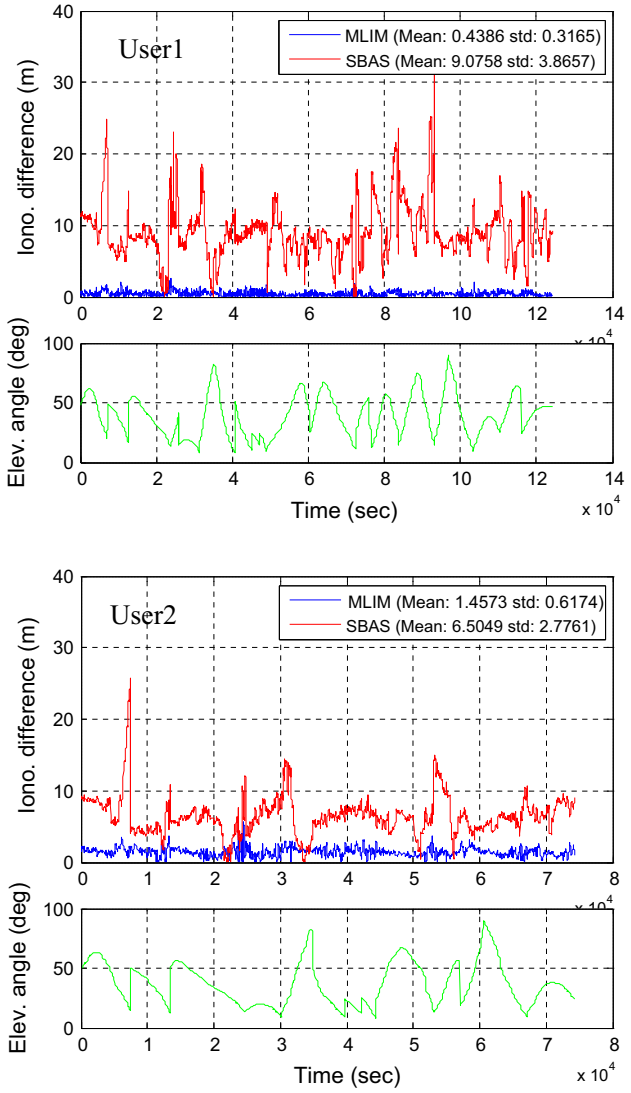

Fig. 13 Ionospheric correction error of the MLIM and MSAS ionospheric model

model has higher accuracy and better fitting ability of the estimated ionospheric delay compared to the MSAS. For User 2, the proposed ionospheric delay model gives poor corrections for low elevation angles, but still has higher accuracy compared to that of the SBAS ionospheric model. The poor corrections are caused by the large OF error at low elevation angles. The large OF error leads to errors in delay conversion. For User 1, the proposed ionospheric delay model provides stable and accurate corrections because the user is close to SRS. The ionospheric delay for User 1 is similar to that at SRS. The correction value after WLS is almost the same as that at SRS. A user close to one of these RSs will thus have very accurate and stable ionospheric corrections. Finally, the user can apply the accurate ionospheric corrections from the proposed ionospheric delay model to calculate the ionospheric delay.

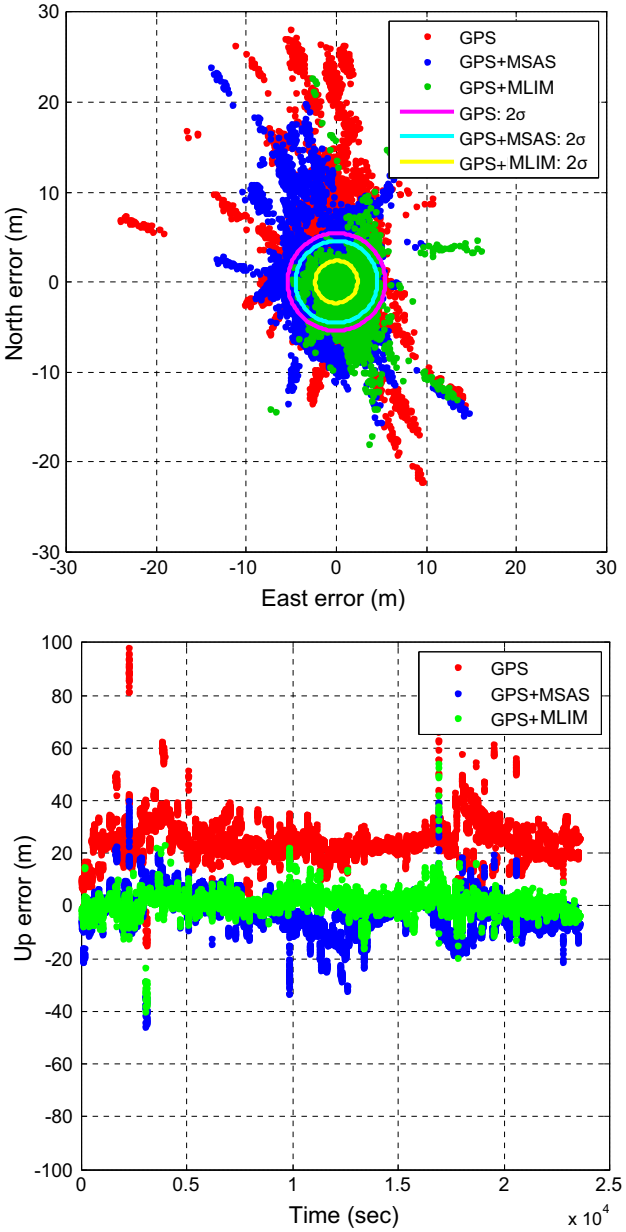

Fig. 14 Comparison of User 1 positioning results obtained using standalone GPS (GPS), MSAS ionospheric correction (GPS + MSAS), and proposed ionospheric model (GPS + MLIM)

Comparison of user positioning performance

The user positioning performance for each ionospheric delay model is analyzed in this section. Figures 14 and 15 show comparison plots of the positioning results for users 1 and 2 based on different ionospheric delay models, respectively. In these two figures, the red, blue, and green lines are the positioning results obtained using standalone GPS only, MSAS ionospheric correction, and the proposed ionospheric model, respectively. All the positioning results are compared to the true locations of users. The mean and

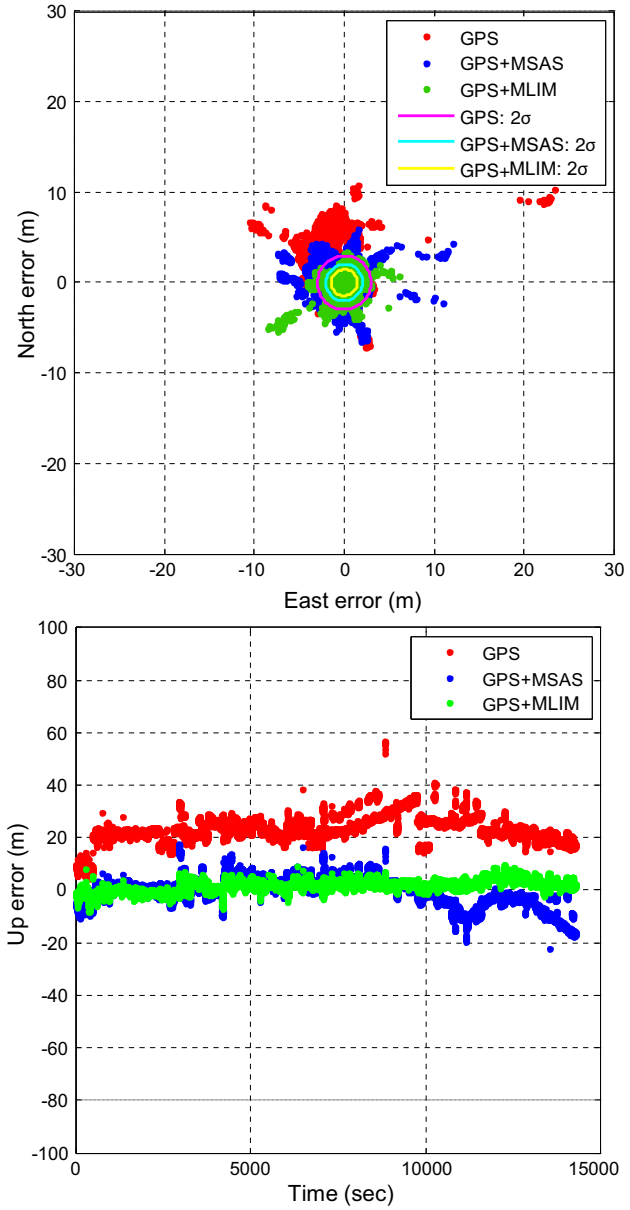

Fig. 15 Comparison of User 2 positioning results obtained using standalone GPS (GPS), MSAS ionospheric correction (GPS + MSAS), and proposed ionospheric model (GPS + MLIM)

standard deviations of the three error indices are summarized in Tables 4 and 5, respectively. The results show that the user positioning performance is improved by both the MSAS ionospheric model and the proposed ionospheric model. Importantly, the proposed ionospheric delay model has better accuracy than that of the MSAS ionospheric model. As a result, the mean values of the positioning results are closer to the true user location after applying the proposed model. The standard deviation shows that the proposed ionospheric model has better capability of removing noise from the ionospheric delay compared to the

Table 4 Mean values of positioning results obtained using standalone GPS, MSAS correction, and MLIM

	Horizontal	Vertical	RMSE
GPS User 1	4.00	24.58	25.21
GPS User 2	3.87	23.37	22.87
MSAS User 1	0.91	−1.72	6.06
MSAS User 2	0.42	−0.35	3.42
MLIM User 1	0.91	1.42	3.84
MLIM User 2	0.11	1.82	3.42

Units are in meters

Table 5 Standard deviations of positioning results obtained using standalone GPS, MSAS correction, and MLIM

	Horizontal	Vertical	RMSE
GPS User 1	4.15	5.73	6.01
GPS User 2	2.56	5.18	4.94
MSAS User 1	3.86	6.13	4.75
MSAS User 2	1.56	5.41	3.48
MLIM User 1	1.73	3.04	3.91
MLIM User 2	1.24	2.17	2.64

Units are in meters

MSAS ionospheric model. The results show that the proposed ionospheric delay model provides good positioning performance and accurate ionospheric delay corrections for users in this region.

Verification of the correction under the severe ionospheric activity

This section verifies the data of October 2, 2013, during a severe ionospheric storm. The user positioning performance for different ionospheric delay model is analyzed in Fig. 16. The positioning results are also divided into standalone GPS, MSAS ionospheric correction, and the proposed ionospheric model. The mean and standard deviations of the error are summarized in Tables 6 and 7. The Kp values for October 2, 2013, indicate that the GPS user is facing an ionospheric storm. In this situation, the MSAS ionospheric grid model hardly provides any useful correction in horizontal positioning. Although the mean value of the vertical positioning result becomes better, the standard deviation displays the MSAS correction brings more noise to the user.

Compared to the MSAS ionospheric model, the proposed ionospheric model removes the severe ionospheric delay as suggested by the statistical result and the corresponding horizontal and vertical positioning results are

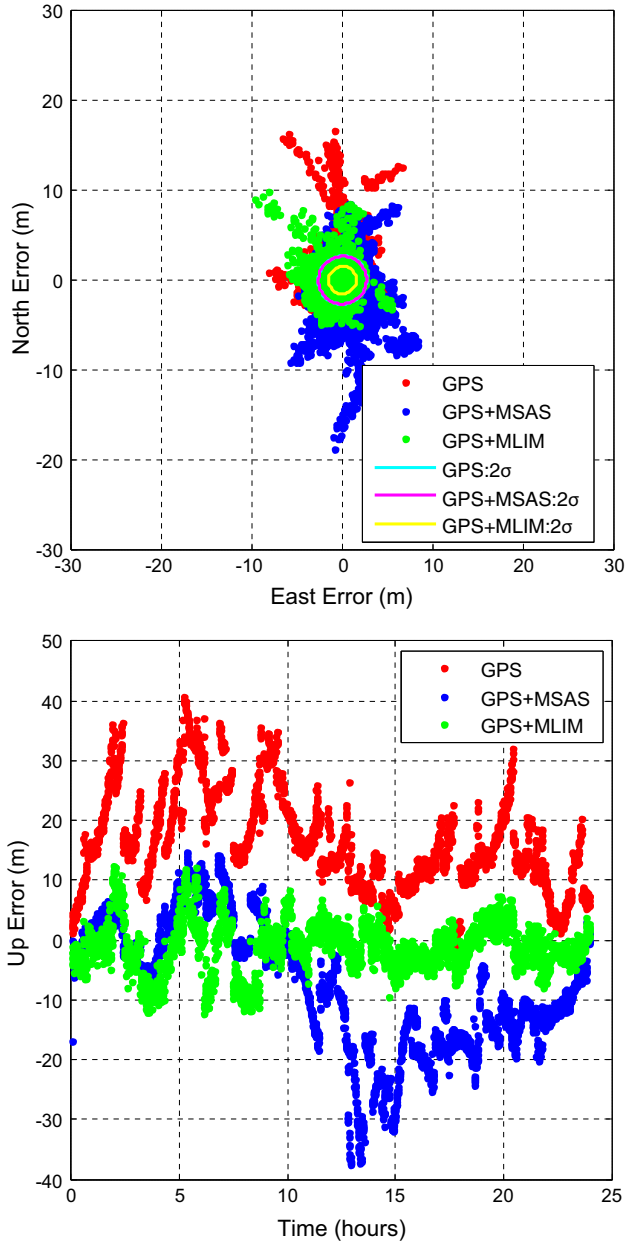

Fig. 16 Comparison of second experiment positioning results obtained using standalone GPS (GPS), MSAS ionospheric correction (GPS + MSAS), and MLIM (GPS + MLIM)

Table 6 Mean values of positioning results obtained using standalone GPS, MSAS correction, and MLIM

	Horizontal	Vertical	RMSE
GPS user	3.15	16.36	16.86
MSAS user	4.27	−7.63	11.85
MLIM user	2.07	−1.15	4.28

Units are in meters

Table 7 Standard deviations of positioning results obtained using standalone GPS, MSAS correction, and MLIM

	Horizontal	Vertical	RMSE
GPS user	2.66	8.25	8.28
MSAS user	2.68	10.74	7.66
MLIM user	1.55	4.17	2.66

Units are in meters

more accurate. As a result, the proposed ionospheric delay model provides accurate ionospheric delay corrections for the user under unstable ionospheric activity.

Conclusions

A wide-area ionospheric delay model for users in the Asia-Pacific region was developed. Real GPS data collected from several RSs and users in Taiwan, South Korea, Japan, and China were used to validate the wide-area ionospheric delay corrections of the proposed ionospheric delay model. The MSAS ionospheric grid model was used to check the validity of the ionospheric delay values. The proposed model and its simplified version were compared. The user positioning results obtained using only GPS were improved by the proposed ionospheric delay model under both nominal and disturbed ionospheric conditions. The high accuracy and resolution of the proposed ionospheric delay model for wide-area users were thus validated.

In order to increase the applications of the proposed model, such as for mobile users, a simplified model was proposed. The simplified ionospheric delay model provided almost the same performance as that of the original proposed model while reducing the computational burden. Finally, a selection mechanism between the original proposed ionospheric delay model and its simplified version was developed. This extended the applicability of this proposed ionospheric delay model.

Acknowledgments This work was supported by the College of Engineering at National Cheng Kung University and the National Science Council of Taiwan under Grant NSC 101-2628-E-006-013-MY3. The authors gratefully acknowledge this support.

References

Allain DJ, Mitchell CN (2010) Comparison of 4D tomographic mapping versus thin-shell approximation for ionospheric delay corrections for single-frequency GPS receivers over North America. GPS Solut 14(3):279–291

Bartels J (1949) The standardized index Ks and the planetary index Kp, IATME Bull 126, 97. IUGG Publ. Office, Paris

Chao YC, Tsai YJ, Evans J, Kee C, Walter T, Enge PK, Powell JD and Parkinson BW (1996) Generation of ionospheric correction and confidence estimates for WAAS. In: Proceedings ION AM 1996, Institute of Navigation, June 19–21, Cambridge, Massachusetts, pp 139–146

Chen CH, Jan SS (2008) Performance Assessment of a Local Area Monitoring System in Asia Pacific Region. In Proceedings ION GNSS 2008, Institute of Navigation, September 16–19, Savannah, Georgia, 1962–1970

Enge P (2001) Global positioning system: signals, measurements, and performance. Ganga-Jamuna Press, Lincoln

Gurtner W (2007) RINEX—the receiver-independent exchange format Version 3.00, Astronomical Institute, University of Bern, November 28

Hatch RR (1982) The synergism of GPS code and carrier measurements. In: Proceedings of the third geodetic symposium on satellite doppler positioning, Las Cruces, New Mexico

Kan ST (2005) Analysis of the satellite based augmentation system in Taiwan with an emphasis on ionosphere modeling. Department of Aeronautics and Astronautics Thesis, National Cheng Kung University

Macalalad EP, Tsai LC, Wu J, Liu CH (2013) Application of the Taiwan Ionospheric Model to single-frequency ionospheric delay corrections for GPS positioning. GPS Solut 17(3):337–346

Parkinson BW and Spilker JJ (1996) Global positioning system: theory and application, American Institute of Aeronautics and Astronautics

Radicella SM and Nava B (2002) Study of the obliquity factor error in slant to vertical and vertical to slant ionospheric delay conversion. In: Proceedings of the XXVIIth URSI General Assembly in Maastricht

Radicella SM, Nava B, Coïsson P, Kersley L and Bailey GJ (2004) Effects of gradients of the electron density on earth-space communications. Annals of geophysics, Supplement to Vol. 47, N. 2/3

Tsai YJ, Chao YC, Walter T, and Kee C (1995) Evaluation of orbit and clock models for real-time WAAS. Proc. ION NTM 995, Institute of Navigation, January 18–20, Anaheim, California, pp 539–547

WAAS MOPS (2006) Minimum operational performance standards for global positioning system/wide area augmentation system airborne equipment, RTCA/DO-229D

An-Lin Tao is a Ph.D. candidate in the Department of Aeronautics and Astronautics at National Cheng Kung University (NCKU), Taiwan. He received his B.S. and M.S. degrees in Aeronautics and Astronautics from NCKU in 2009 and 2011, respectively. His research currently focuses on the development and analysis of the Global Navigation Satellite System (GNSS) ionospheric model.

Shau-Shiun Jan is an Associate Professor of the Department of Aeronautics and Astronautics, NCKU, Taiwan. He directs the NCKU Communication and Navigation Systems Laboratory (CNSL). His research focuses on GNSS augmentation system design, analysis, and application. He received his Ph.D. degree in Aeronautics and Astronautics from Stanford University in 2003.